Meteorol. Atmos. Phys. 44, 63–83 (1990)

Meteorology and Atmospheric Physics

551.509.33:551.515.5

Department of Meteorology, Florida State University, Tallahassee, Florida, U.S.A.

Predictability of Low Frequency Modes

T. N. Krishnamurti, M. Subramaniam, D. K. Oosterhof, and **G. Daughenbaugh**

With 16 Figures

Received October 16, 1989
Revised November 20, 1989

Summary

In this paper we propose a procedure for the extended integration of low frequency modes of the time scale of 30 to 50 days. A major limitation of the extended integrations arise from a contamination of low frequency modes as a result of energy exchanges from the higher frequency modes. In this study we show an example on the prediction of low frequency mode to almost a month which is roughly 3 weeks beyond the conventional predictability. This was accomplished by filtering the higher frequency modes from the initial state. The initial state included a time mean state and a low frequency mode. The sea surface temperature anomalies on this time scale and the annual cycle were also prescribed.

The specific experiment relates to the occurrence of a dry and a wet spell in the monsoon region. The meridional passage of an anticyclonic circulation anomaly over the lower troposphere and the eastward passage of a negative velocity potential anomaly over the upper levels of the Indian monsoon, on this time scale, are reasonably predicted. The aforementioned experiment was carried out with the 1979 data sets of the global experiment. A second example during an anomalous southward propagation of the low frequency waves over the Indian monsoon region during 1984 was also reasonably predicted by this model. Suggestions for further experimentation on the predictability of low frequency modes are proposed.

1. Introduction

Observations have shown the presence of low frequency motions on the time scale of roughly 30 to 50 days. There are several regional and global aspects of these oscillations that have been emphasized in recent literature. Among these we shall be addressing the following four observational aspects of low frequency motions on the time scale of 30 to 50 days.

a) Meridionally propagating 30 to 50 day waves in the lower troposphere of the monsoon region: This appears as a family of trough-ridge systems that can be seen on the streamline-isotach charts of the time filtered motion field. The passage of a trough or a ridge line over central India generally coincides with the occurrence of a wet or a dry spell respectively. The meridional scale of this system is roughly 2 000 to 3 000 kilometers. The speed of meridional motion is roughly 1° latitude/day (Krishnamurti and Subrahmanyam, 1982; Yasunari, 1980, 1981). During certain years, the meridional motion and passage of these systems during the summer monsoon season is quite regular while in other years the motion is somewhat irregular. The reasons for this type of interannual behavior are not quite clear at the present time (Mehta and Krishnamurti, 1988).

Figure 1 illustrates a sequence of 850 mb wind field in the time scale of 30 to 50 days; this is based on analyzed data sets. This sequence illustrates the meridional passage of a counter clockwise circulation anomaly across India. The starting date of this sequence is July 31, 1979 12 UTC. (A list of acronyms appears in Table 1.) Maps are shown at intervals of 5 days and cover a 35-day period. This panel of charts covers the period of a dry

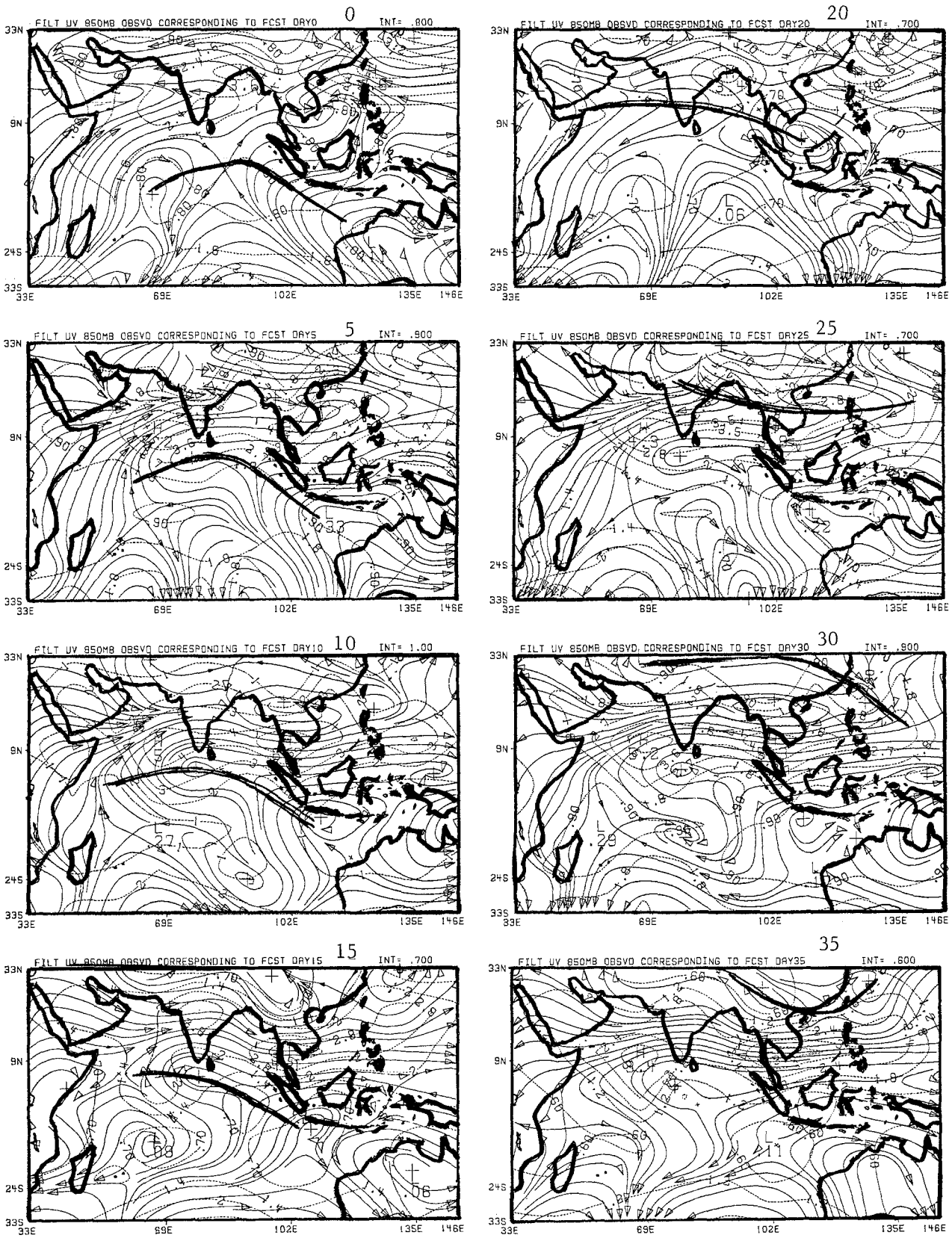

Fig. 1. 30- to 50-day time filtered flow field at 850 mb from July 31 through September 4, 1979 (at intervals of 5 days). Based on observations, streamlines, solid lines, isotachs dashed, units ms^{-1}

Table 1. *List of Acronyms*

ECMWF	European Center for Medium Range Weather Forecasts
FGGE	First GARP (Global Atmospheric Research Program) Global Experiment
FSU	Florida State University
NASA-GLAS	National Aeronautical Space Administration – Goddard Laboratory for Atmospheric Sciences
NMC	National Meteorological Center
NOAA	National Oceanic and Atmospheric Administration
NSF	National Science Foundation
SST	Sea Surface Temperature
SSTA	Sea Surface Temperature Anomaly
UTC	Universal Time Coordinate

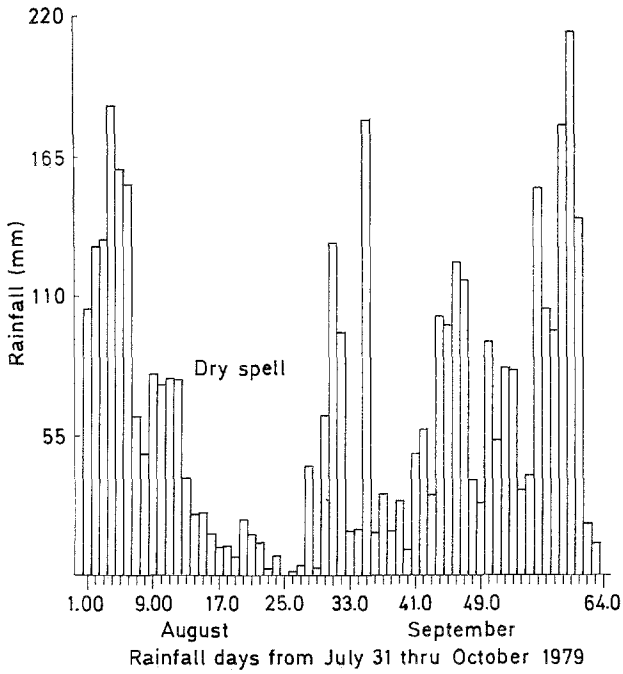

Fig. 2. Histogram of daily rainfall (mm/day) over central India during August and September of 1979

spell of the Indian monsoon that is illustrated in Fig. 2 from histograms of daily rainfall over central India during the summer of 1979. The dry spell during August is of interest for the present study. The low frequency counterclockwise circulation propagates from roughly the equator to 30°N during this period. The speed of meridional propagation was somewhat variable during this period. An objective of this study is to predict the meridional propagation of this wave.

b) Zonally propagating planetary scale divergent circulations on this time scale: During this period at 200 mb the eastward propagating divergent wave was clearly evident. A sequence of charts of the velocity potential (on the time scale of 30–50 days) at 200 mb, for this period, at interval of 5 days, are shown in Fig. 3. The shaded areas denote regions of divergent outflows. The FGGE year exhibited a rather pronounced zonal propagation of the divergent wave. The entire FGGE year history of propagation of this wave can be illustrated on a single x-t diagram, following Mehta and Krishnamurti (1988). Figure 4 shows the passage of this wave based on meridionally averaged daily fields of the velocity potential on this time scale. The wave was quite active over most of the FGGE year. In early September 1979, during the dry spell over the Indian monsoon region, the passage of a negative anomaly coincided with the passage of a planetary scale convergence field at 200 mb, on this time scale. An objective of this study was to predict the eastward passage of the wave during this dry spell. The dominant scale of the planetary scale divergence is in wave numbers 1 and 2. They traverse the globe, from west to east in roughly 30 to 50 days. The largest amplitude is in the equatorial latitudes. The divergent circulations cover a large span of latitudes. They can be seen even as far as 35°N and 30°S. These broad, divergent circulations appear to be related to equatorial and monsoonal heat sources and sinks (Lorenc, 1984; Krishnamurti et al., 1985). The interannual variability of these eastward propagating waves have been studied by several authors, and it is noted that the propagations can be somewhat irregular during some of the years (Mehta and Krishnamurti, 1988).

The aforementioned fields based on FGGE IIIb analysis were obtained using a first order Butterworth filter for the entire year of the motion field at the respective levels. The width of the filter used in these illustrations covered the period range of 30 to 50 days. It must be stated that this phenomenon is quite robust and the results shown above remain practically unaltered with the deployment of filters covering a period range of 20 to 60 days of 30 to 60 days (Mehta and Krishnamurti, 1988).

c) An important aspect on this time scale is the air-sea interaction: We have recently examined the

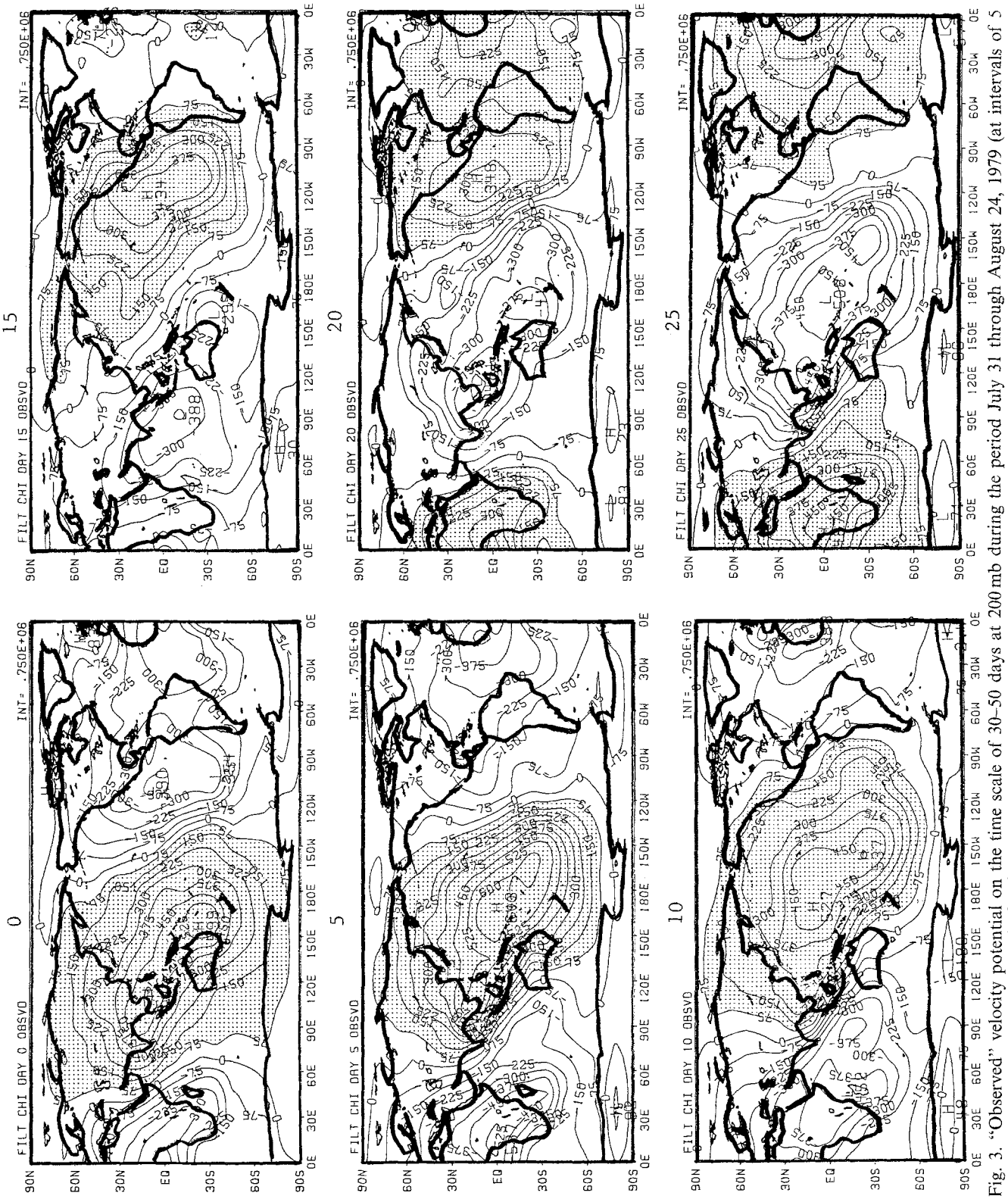

Fig. 3. "Observed" velocity potential on the time scale of 30–50 days at 200 mb during the period July 31 through August 24, 1979 (at intervals of 5 days). Interval of analysis 75×10^4 m^2 s^{-1}

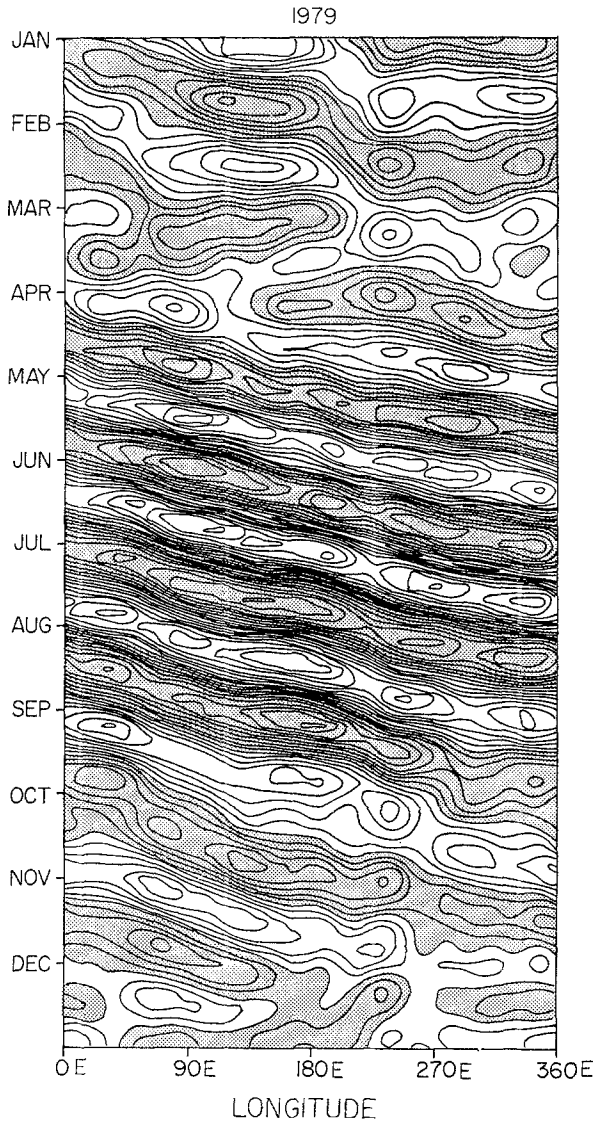

Fig. 4. An x-t diagram of the 200 mb velocity potential meridionally averaged from 10°S to 10°N showing the prominent eastward motion of the divergent wave. Interval $m^2 s^{-1}$. Shaded area denotes negative values

oceanic fluxes of sensible and latent heat on this time scale (Krishnamurti et al., 1988 b). When fluxes are calculated using the so-called "surface similarity theory", the basic variables are the SST, the surface wind, the temperature and humidity at the top of a constant flux layer. The similarity fluxes are defined from expressions that invoke the Monin-Obukhov length and a non-linear coupling of the momentum, heat and moisture fluxes. Because of this non-linear coupling, one can diagnose the relative importance of the low frequency variations of SST, surface wind, air temperature and humidity and assess their role in the contribution to fluxes on this time scale. A detailed diagnostic study was recently completed by Krishnamurti et al. (1988 b). It was found that the latent heat flux variations on the time scale of 30 to 50 days can be as large as 10 to 20 watts/m^2, which was about 5 to 10% of the total flux over the Indian and Pacific oceans. It was also noted that wind variation on this time scale was an important contributor; next in line are the contributions from SST variations on this time scale. The variations in air temperature and humidity were relatively less important. Although the amplitude of SST variations was only of the order of 0.8 to 1 °C on this time scale, that coupled with wind variations of the order 3 to 5 ms^{-1} contributed to significant latent heat fluxes, i.e., $\approx$ 10 to 20 watts/m^2. The sign of these low frequency fluxes are preserved for a couple of weeks, thus their role can become quite significant.

d) Another observational aspect relevant to this problem is the energy exchange in the frequency domain: The maintenance of low frequency modes has been addressed via detailed computations of energetics in the frequency domain using daily globally analyzed data sets covering many years (Sheng, 1986). These studies are somewhat analogous to the estimates of energetics in the zonal wave number domain (Saltzman, 1970). In the latter approach, one speaks of kinetic energy exchanges from zonal flows to eddies of certain scales, and of waves to waves via nonlinear interactions. This includes interactions in the wave number domain among potential and kinetic energy over differnt scales. In the frequency domain, analogous selection rules govern the exchanges of energy. Here one can partition the temporal domain among long-term mean, and low and high frequency motions. In the frequency domain, the kinetic to kinetic energy exchanges can occur among long-term time mean flows and other frequencies, or among triads of frequencies (analogous to the wave number domain), i.e., an interaction among frequencies ν_n, $(\nu_n \pm \nu_m)$ and ν_m can result in loss or gain of energy for the intermediate frequency ν_m. This exchange of energy is analogous to energy exchanges in the wave number domain. The potential to kinetic energy exchanges are restricted to occur at the same frequencies as in the wave number domain where potential to kinetic energy exchanges are restricted to occur at the same wave numbers.

The results of such energetics calculations, performed by Sheng (1986), show that the kinetic energy of low frequency modes on the time scale of 30 to 50 days are maintained by the following processes:

i) They receive a substantial amount of kinetic energy from the high frequencies;

ii) they gain kinetic energy from the long-term time mean flow;

iii) they receive a smaller amount of energy from the potential energy on the same frequencies.

Figure 5, following Sheng (1986), shows the energy gained by different frequency intervals from the aforementioned kinetic to kinetic energy exchange in the frequency domain. In the period range (shown along the abscissa) of interest here (around 30 to 50 days) this energy exchange in the frequency domain results in a gain of energy. The higher frequencies clearly lose a substantial amount of energy by this process. The annual cycle also loses energy to other frequencies. This was a rather robust result and has ben substantiated by the data sets for a six-year period.

A rapid loss of predictability of low frequency modes in real data long-term integrations have been noted at ECMWF and at NMC. Dr William Heckley, of the ECMWF (personal communication), examined the presence (or absence) of the monsoonal low frequency modes from several ensembles of predicted data for the FGEE period. The zero day ensemble of 365 days is a string of the initialized FGGE data set. This string, as expected, contained the meridionally propagating low frequency modes. However, as the strings of the ensembles of 1, 2, 3, 4, and 5 day forecasts were examined separately, in this context, it was noted that the low frequency modes were lost by about day 5. Figure 6 illustrates the strategy for these experiments. The ensemble of 0, 1, 2, 3, 4, and 5 day forecast strings based on 365 operational forecasts showed that the low frequency mode was absent in the 5-day string. Dr T. C. Chen, Iowa State (personal communication), carried out a similar set of calculations from ensembles of NMC global forecasts and basically confirmed the same results. The predictability of the low frequency modes appears to be somewhat limited. Although global models tend to show features of the low frequency modes in their long-

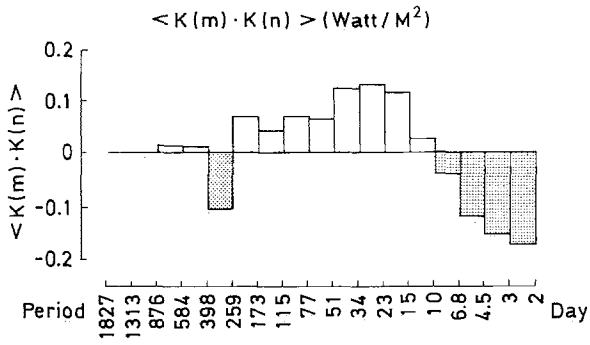

Fig. 5. Kinetic to kinetic energy loss or gain for different frequencies during 1980 through 1985. Units m^{-2} (based on Sheng, 1986)

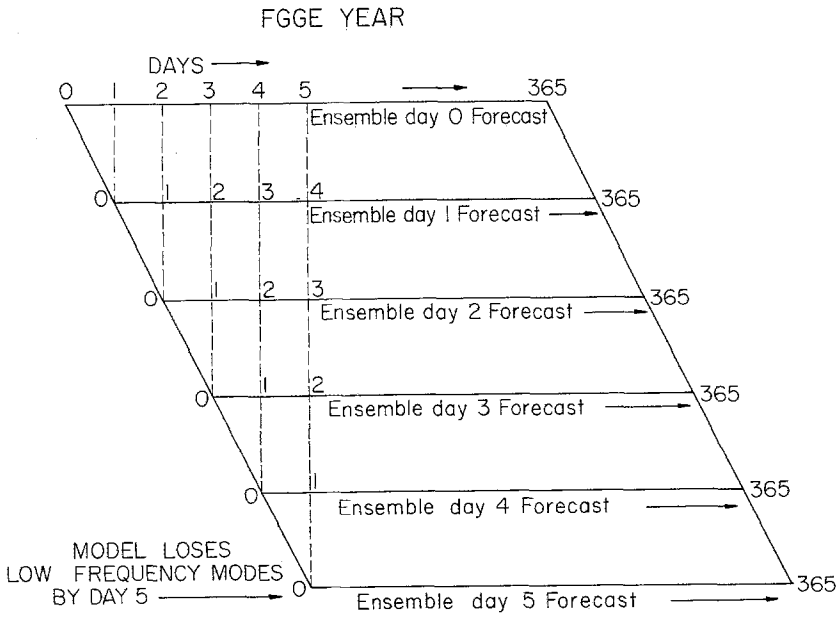

Fig. 6. Schematic outline of the ensembles of 0-, 1-, 2-, 3-, 4-, and 5-day forecasts during 1979

term integrations, the precise prediction of their phase and amplitude beyond day 5 does not seem possible from straightforward integrations. This loss of predictability, we believe, occurs from a contamination due to the error growth in the prediction of high frequency modes. We furthermore believe that the transfer of energy to these low frequency modes conveys errors rather quickly. It has been suggested (Dr M. M. Navon, FSU, personal communication) that the loss of predictability of low frequency modes can also arise from the errors in the time differencing schemes. Second order accurate time differencing schemes may lose accuracy in predicting the small time tendencies of these low frequency modes, arising largely from the inherent truncation errors. Dr Navon ran two long-term integrations of a NASA-GLAS global model with second and fourth order accurate time differencing schemes. The monthly mean flows were substantially different in these two integrations. This is an area that deserves further research with reference to the predictability of low frequency modes. The conclusion was drawn that the global model has a predictability, for the low frequency modes, of about 4 to 5 days. Deficiencies of second order accurate time differencing schemes have been addressed by Browning et al. (1989). A systematic analysis of the higher order time differencing in this context deserves further work.

We feel strongly that this loss of predictability for the low frequency modes arises largely due to the errors the model makes in the prediction of the higher frequency motions. The latter contaminate the low frequency modes by the transfer of errors via these energy exchanges.

2. Proposed Experiments

The aforementioned observations and ideas were useful in the design of a class of long-term integration experiments where we have made an effort to extend the predictability of low frequency modes. All of the experiments described here were carried out with a global spectral model which utilizes a horizontal truncation of 21 waves (Triangular i.e., T21). The FSU global model is described in Appendix I.

Specifically, we have designed the following experiments:

2.1 The Control Experiment

This experiment was carried out with a comprehensive global spectral model (Krishnamurti and Oosterhof, 1989) where the model was initialized using nonlinear normal mode initialization using global data sets for July 31, 1979 (1200 UTC). This experiment included an annual cycle of SST. The annual cycle of the SST was based on merged monthly mean SST fields for the year 1979. A 270-day integration was carried out starting from that day. (This was a conventional forecast experiment.)

2.2 The Anomaly Experiment

It was felt that one could perhaps delay the contamination of the low frequency mode by suppressing the high frequency modes entirely in the initial state. The inclusion of a time mean state (for all vertical levels and for all variables) and the phase and amplitude of the low frequency mode at the initial time was considered necessary. Furthermore, it was felt that air-sea interaction, on this time scale, had to be retained by prescribing appropriate SST anomalies and the annual cycle of the SST. The premise of this experiment was to see if one or two cycles of the passage of a low frequency wave could be handled by such a model prior to its contamination as the higher frequency motions evolve. The choice of a lower resolution model was deliberate since it was felt that it would not quickly excite very large amplitude transient storms at the higher frequencies. The initial state was obtained as follows:

i) A time mean state was obtained for all variables at all vertical levels using the data sets for a 47-day period preceding the initial date (i.e. July 31, 1979, 12 UTC). Figure 7 shows the vertical discretization of the global model.

ii) A low frequency mode for the initial date was based on the data sets for the preceding 270-day period utilizing in a time filter analysis. A Butterworth filter was used for this purpose (see Appendix II). It was carried out at each of the transform grid points at all of the vertical levels for all of the basic variables.

iii) SST anomalies on the time scale of 30 to 50 days. These were updated during the course of integration. The data sets for the SST anomalies, on the time scale of 30 to 50 days, used in the present study are described in Krishnamurti et al.

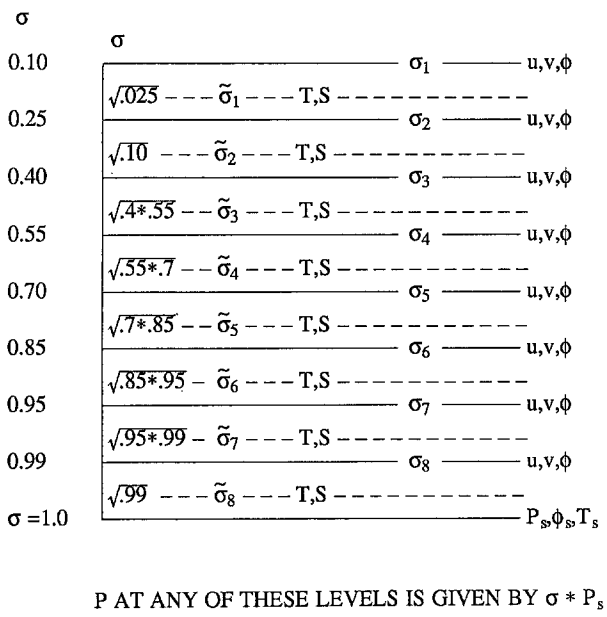

Fig. 7. Vertical descretization of the FSU global spectral model

(1988 b). This is a global data set based on ECMWF's FGGE analysis. In the anomaly experiment the daily values of these time filtered SST data sets were added to the annual cycle of the SST.

iv) The annual cycle of SST varies from month to month. These same fields were also used in the control experiment. They were obtained from the monthly mean fields for the year 1979. The daily fields of sea surface temperature (SSTA + Annual Cycle) were updated at the lower boundary during the course of integrations. In that sense this study is not a prediction experiment. Furthermore, following several other studies on the climatic impact of SSTA, we have enhanced the SSTA by a factor of 3.5. This was necessary in the 8 layer global model since it lacked an adequate resolution for the calculation of surface fluxes of moisture, heat and momentum in the planetary boundary layer. The retention of the time mean state and the SST anomalies was to provide one of the other important energy sources for these low frequency modes.

It should be stated that a simple use of normal mode initialization with a frequency cut of to remove the high frequency modes (time scale less than 10 days) does not accomplish this same purpose, since it only affects the divergent wind and any higher frequency modes in the other fields (such as stream function, temperature and pressure) which soon generate divergence fields at the higher frequencies. This is not analogous to the gravity mode initialization problem.

In summary the time means used in the experiment were obtained by taking averaged values of all variables at all vertical levels of the model. Here the mean is taken for a 47-day period (day 119 to day 0) preceding the initial state. Day 0, i.e. the start of the experiment, is July 31, 1979, 12 UTC. The low frequency mode on day 0 is defined from a time filter using the data sets from day -269 to day 0, i.e 270 days. This time filtering is separately carried out for all variables. The SST anomalies were defined from a time filtering of the 10-day averaged SST fields from the ECMWF data files. The period of the basic data included December 1, 1978 through April 30, 1980. The time filtered SST anomalies for the period July 31, 1979 onwards were used in the anomaly experiment. At the start of this experiment, these fields were subjected to a nonlinear normal mode initialization.

3. Results of Experiments

3.1 Monsoonal Lower Tropospheric Meridionally Propagating Waves

Figure 8 a and b illustrate the predicted 850 mb streamline and isotachs of the motion field on the time scale of 30 to 50 days for the control and anomaly experiment respectively. Each of these covers a period of 35 days (at intervals of 5 days). The results shown here are to be compared with Fig. 1 where the results based on observations covering the same period are presented. In this sequence of charts the meridional passage of a ridge line and the occurrence of a dry spell over central and northern India was illustrated (see Figs. 1 and 2). The control experiment fails to capture this passage. The anomaly experiment handles this passage extremely well. The streamlines, on this time scale, for the anomaly experiment very closely resemble those based on observations. The location of the ridge line over the central longitude of India is correctly predicted for almost one month. The meridional passage of the ridge across the

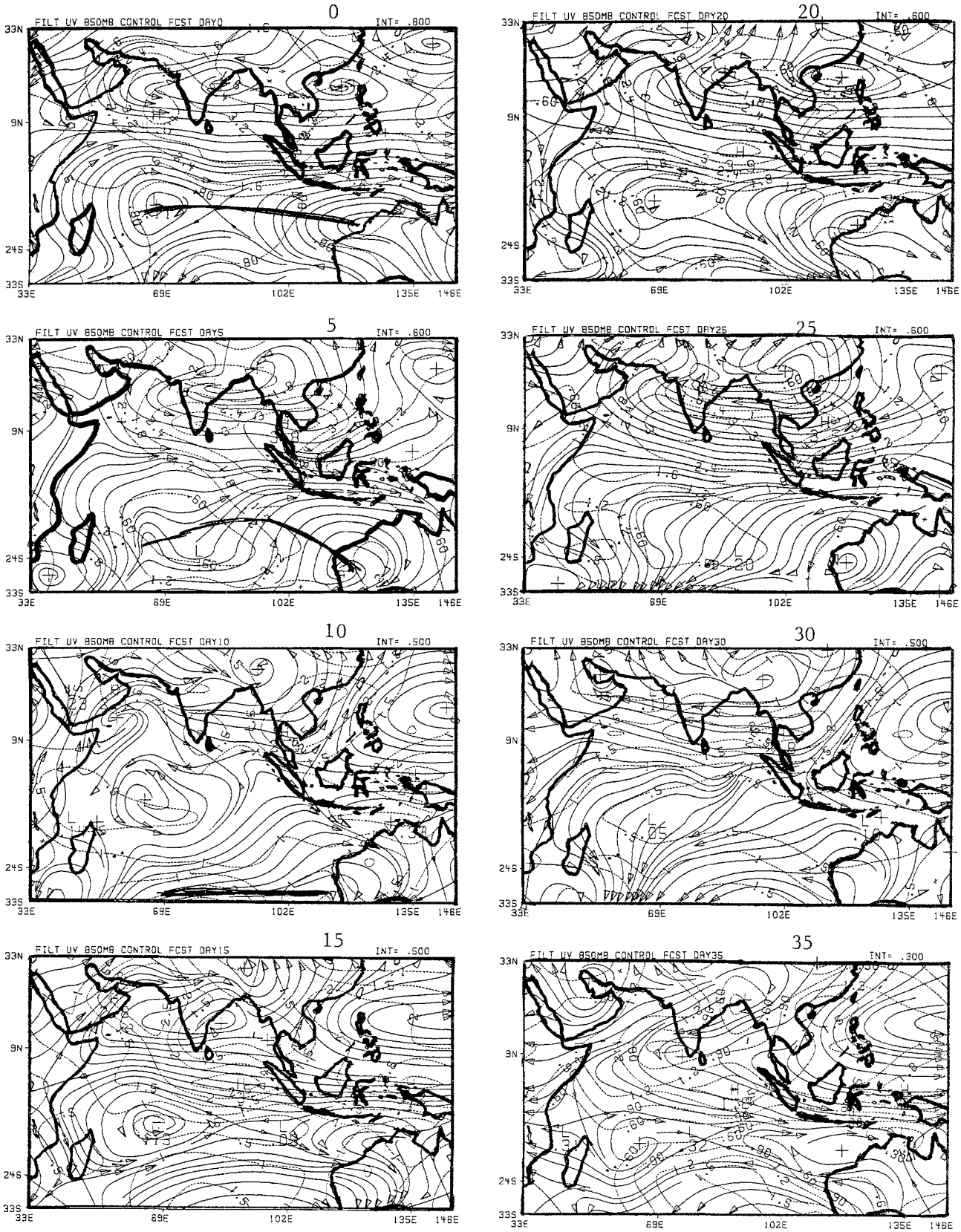

Fig. 8a. 30- to 50-day time filtered flow field at 850 mb from July 31 to September 24, 1979 (at intervals of 5 days). Control experiment-prediction streamlines, solid lines, isotachs dashed, units ms^{-1}

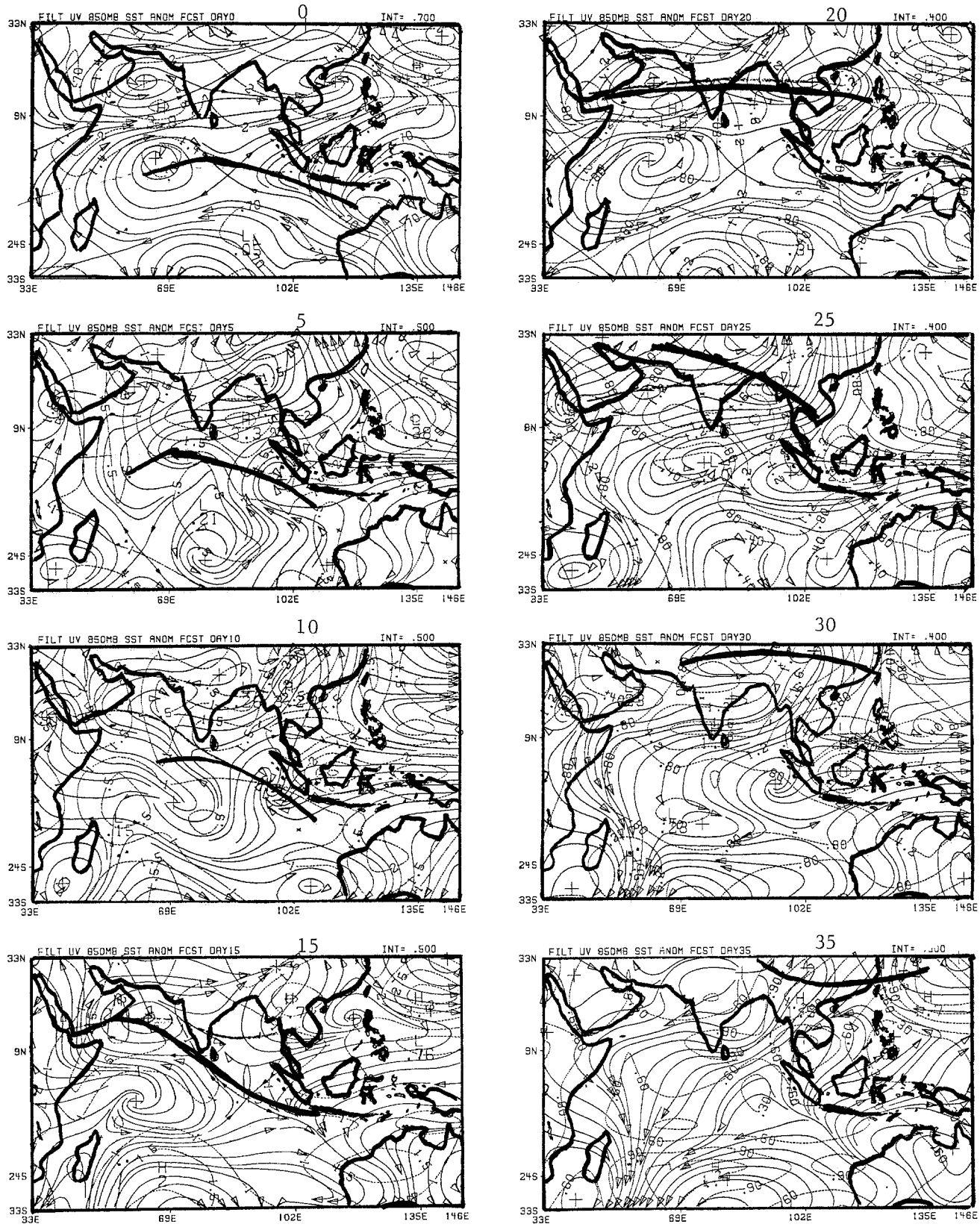

Fig. 8 b. 30- to 50-day time filtered flow field at 850 mb from July 31 to September 24, 1979 (at intervals of 5 days). Anomaly experiment-prediction streamlines, solid lines, isotachs dashed, units ms^{-1}

central longitude of India is shown in Fig. 9. Here one can compare the results based on observations with those from the predictions of the control and the anomaly experiments. The initial position of the ridge lines in the control experiment does not utilize any past information; the initial position of the ridge line for the anomaly experiment is entirely based on past information. Thus the initial locations of the ridge line for the control and the anomaly experiment are displaced with respect to each other. The latter utilizes analysis (of past information) and thus agrees with the "observational" location of the ridge line initially. It appears that the phase speed is predicted very well; however, the amplitude of the low frequency mode is underestimated in this forecast by roughly 50%. Because of the loss of amplitude after the first cycle we feel that this forecast loses its usefulness beyond 30 days.

The growth of higher frequency motions in this anomaly experiment was quite slow. Figure 10 a and b shows the time evolution of zonal velocity, at a selected point, for the anomaly experiment at 850 mb. It shows that the zonal wind oscillations for the first 70 days have a dominant low frequency. It is only after this period that we see the oscillations being dominated by the higher frequencies. The lower panel of Fig. 10 shows the time filtered zonal velocity at that selected point. The amplitude of the low frequency mode falls off after 2 cycles.

The time mean state contains a three-dimensionally varying stratification and wind shear. The

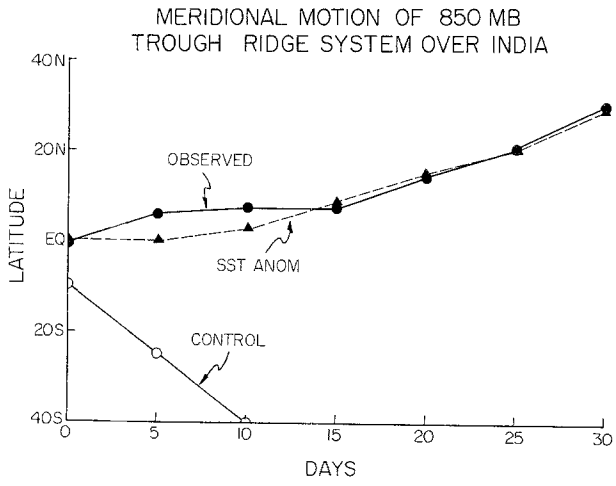

Fig. 9. A y-t diagram of the monsoonal low frequency ridge line at 850 mb. The results based on observation, control and anomaly experiment are shown here

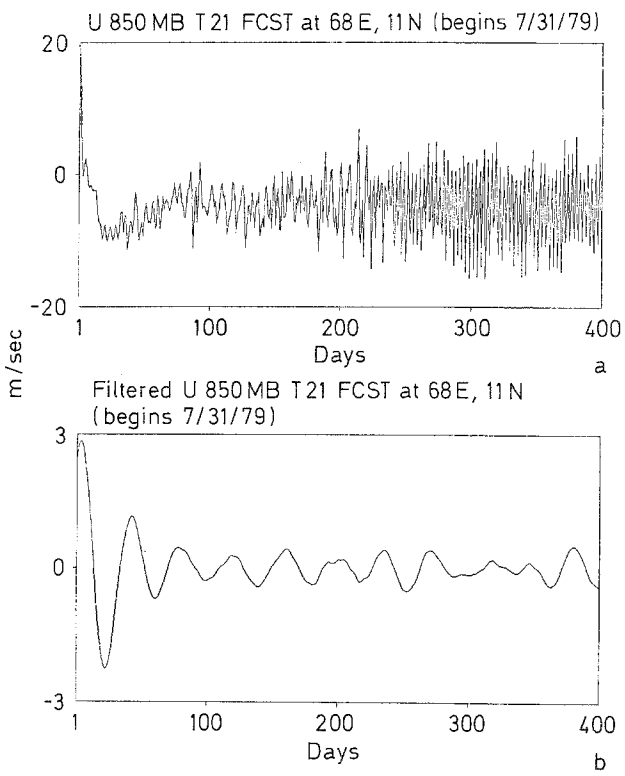

Fig. 10. (Top panel) time history of the zonal wind from the anomaly experiment (ms^{-1}) and (bottom panel) the time history of the time filtered zonal wind

low frequency mode, imbedded within it initially, moves meridionally with a reasonable speed and shape for about 30 days. Knowing that the passage of a ridge coincides with a dry spell, it is possible – at least in this one experiment – to suggest that the occurrence of a dry spell beyond the time scale of conventional predictability, which is of the order of a week, was possible. However, that too was made at the expense of feeding in future values of the SST anomaly at the lower boundary and hence this is not a truly predictive experiment.

3.2 Planetary Scale Divergent Waves in the Upper Troposphere

The velocity potential fields at 200 mb based on observations and those from the control and the anomaly experiments are compared. These are filtered fields on the time scale of 30 to 50 days. The observed eastward motion of a divergent outflow center (shaded) during the 25 days was illustrated in Fig. 3. This center moved eastward from roughly 160 E to the Greenwich Meridian during this period. The control experiment exhibits an

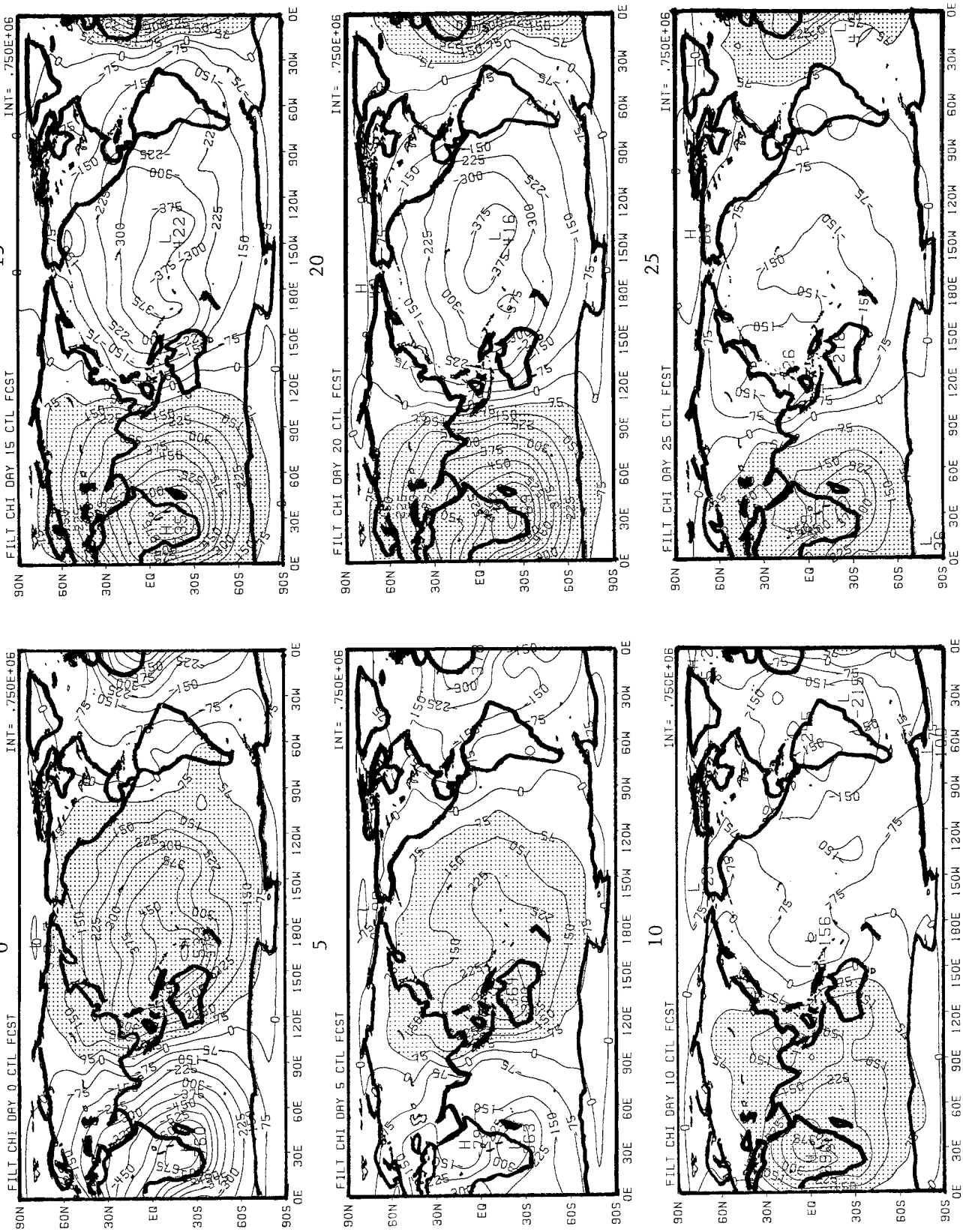

Fig. 11 a. "Control experiment" velocity potential on the time scale of 30–50 days at 200 mb during the period July 31 to August 24, 1979 (at intervals of 5 days). Interval of analysis $75 \times 10^4\,m^2\,s^{-1}$

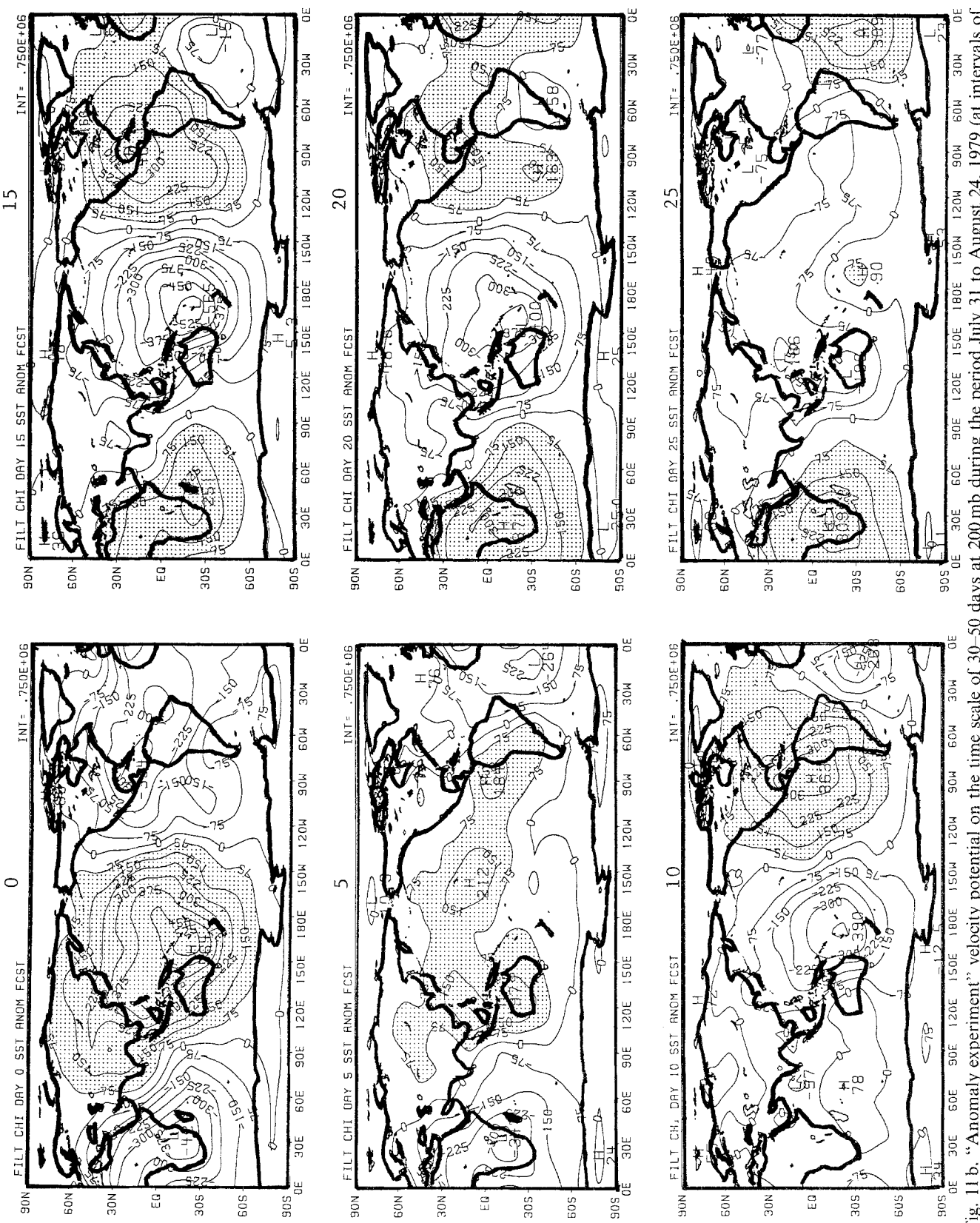

Fig. 11 b. "Anomaly experiment" velocity potential on the time scale of 30–50 days at 200 mb during the period July 31 to August 24, 1979 (at intervals of 5 days). Interval of analysis $75 \times 10^4\ m^2\ s^{-1}$

unusually slow westward movement during the first 10 days and thereafter this center remains stationary over South Africa (Fig. 11 a). It is difficult to assess this peculiar behavior of the low frequency divergent wave in the control experiment. The anomaly experiment shows an eastward propagation of the velocity potential that very closely resembles the "observed" behavior. The predicted phase speed for the anomaly experiment during the 25 days is very close to that seen in Fig. 3. This is better illustrated in Fig. 12 where the eastward motion of the center of the velocity potential anomaly is shown as a function of time. The three curves here show a comparison of the eastward motion for the "observed", the control and the anomaly experiments. The eastward propagation speed was slightly faster for the anomaly experiment during the first 10 days and somewhat slower in the following 10 days as compared to the "observed" phase speed. However, it is clear that a major improvement over the control is realized with the proposed anomaly experiment. Beyond 30 days the phase errors increased. The location of these outflow centers are useful identifiers of tropical convective activity. Hence, we feel that this type of prediction may have some practical usefulness.

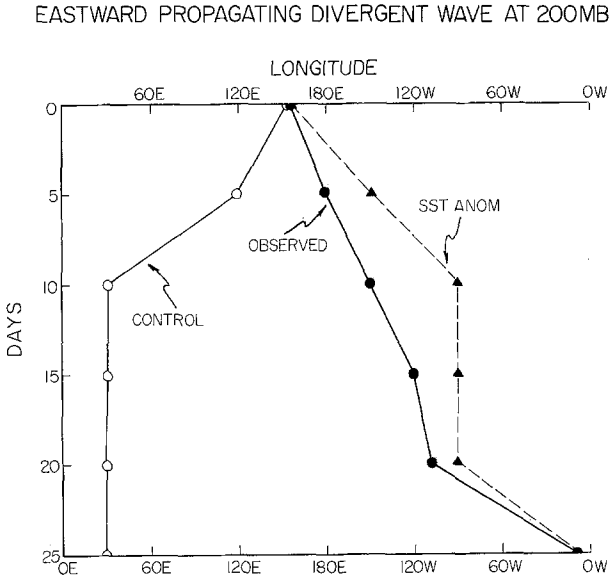

Fig. 12. A y-t diagram of position of the 200 mb divergent center. The results based on observation, control and anomaly experiment are shown here

3.3 Energy Exchange in the Frequency Domain

The computation of the energy exchanges in the frequency domain were carried out for the control and the anomaly experiments. These computations follow the procedure outlined in Appendix III which is based on the work of Sheng (1986). The results of a 270-day integration for the control and anomaly experiment are illustrated in Fig. 13. Here we show the energy gain (or loss) for the different frequencies from nonlinear kinetic to kinetic energy exchanges. Since the high frequency motions were filtered out initially in the anomaly experiments we except a lesser contamination of the low frequency modes from the errors and energy exchanges for the higher frequency motions. The higher frequency motions, as shown in Fig. 10, grow after roughly the second cycle.

The control experiment retains the high frequency modes initially and as a consequence its predictability errors would contribute to a contamination of the low frequency modes from nonlinear energy exchanges. Three sets of curves are

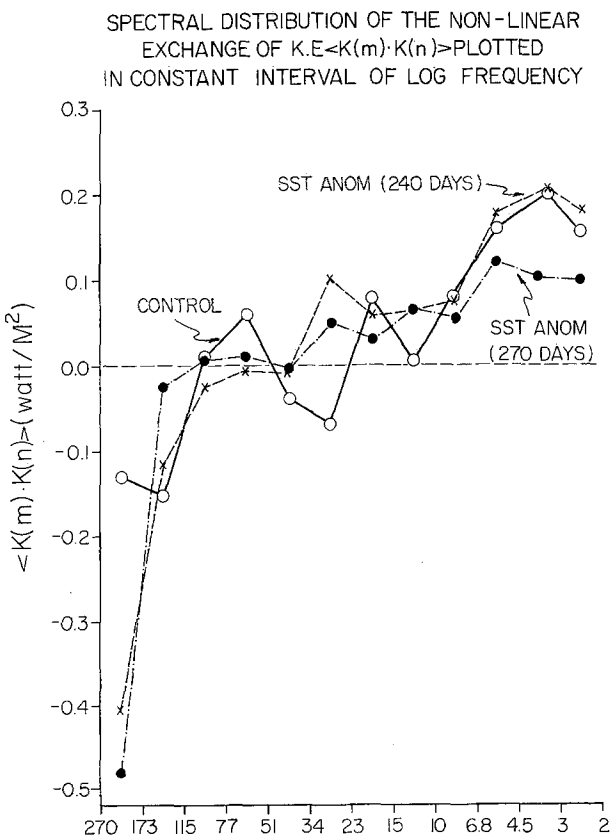

Fig. 13. Kinetic to kinetic energy gain or loss for the control and the anomaly experiments for the 270 day integration. Two calculations for the anomaly experiment are shown, one includes 0 to 270 days, the other covers the period day 31 to day 270

shown in Fig. 13. The period range of about 20 to 50 days shows a loss of energy for the control experiment (shown by the solid line). These frequencies lose energy to all other frequencies, and especially the high frequency motions with periods less than 7 days have the largest net energy gain in the control experiment. The rapid loss of predictability of the low frequency modes may be related to this aspect of the energetics. The results for the anomaly experiment are sums over two periods of integration: days 1 to 270 are shown by the dashed-dotted line and days 31 to 270 shown by the dashed line.

The results for the first 270 days include the first 30-day period during which the phase propagation of the low frequency mode was predicted reasonably by the anomaly experiment. In the anomaly experiment the energy exchange is negligible in the low frequency modes for periods 30 to 50 days. Small amounts of energy are gained by motions with periods larger than 50 days and by those with periods less than 115 days. Motions with periods less than 30 days all exhibit a gain in kinetic energy from their interactions with the other time scales, and they show an increasing trend towards higher frequencies. However the energy gained especially in the frequency range for periods smaller than 6 days is only about half of that of the control experiment. The dashed curve labeled 240 days excludes the first 30-day period during which the predictability of lower frequency modes was high. This averaging shows that all the lower frequency modes with period larger than 30 days encountered a loss in energy and the modes with period less than 30 days experienced a gain of energy from the nonlinear energy exchange process. Also, their gain was higher than that was found when the first 30 days were included. This shows that, once we start integrating the model, high frequency modes develop and amplify by gaining energy from the low frequency modes via the nonlinear wave-wave energy exchanges. As the high frequency modes amplify, the low frequency modes degenerate and get contaminated by the high frequency modes. The energy exchange calculations reveal that for the control experiment and the anomaly experiment excluding the first 30 days, the energy gain by high frequency motions are almost similar and they are approximately twice the energy gain for the same frequency range in the anomaly experiment. This suggest that the rate of contamination of the system by high frequency modes depends on the amplitudes of these modes in the initial field of integration.

3.4 A Second Example

We selected a second example from our observational studies covering the month of August 1984 (Mehta and Krishnamurti, 1988). During this month the low frequency waves on the time scale of 30 to 50 days exhibited an unusual motion both in the lower and the upper troposphere. A trough line on this time scale at 850 mb moved southward from around July 31, 1984. It moved from 25°N to near the equator in the next 30 days. Figure 14 a illustrates the position of the trough line based on the analyzed "observed" data.

An anomaly experiment was designed to parallel the 1979 experiment with a similar definition for the time mean flow, the initial low frequency modes and the SST anomaly. The initial state for the experiment was July 31, 1984, 00 UTC. The predicted positions of the low frequency ridge line

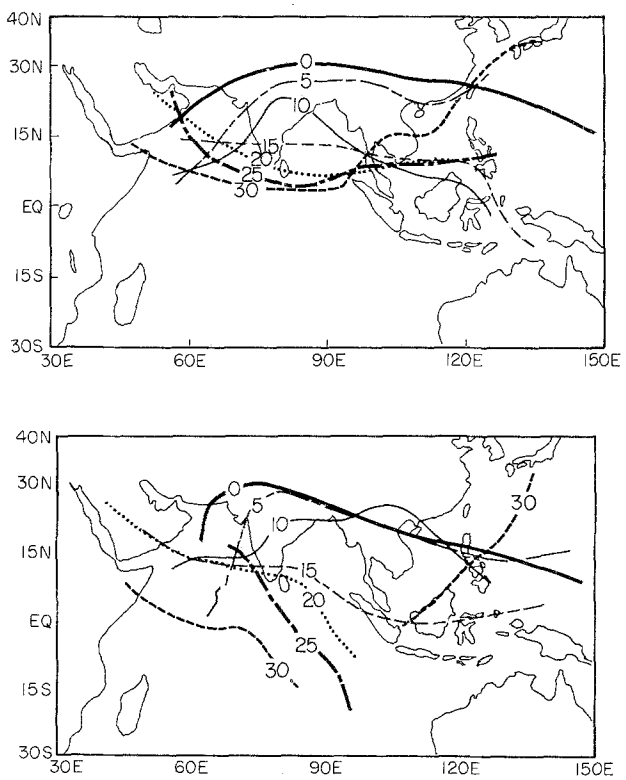

Fig. 14. (Top panel) position of the 850 ridge lines of the time filtered motion field based on "observation" during July 31 to August 29, 1984. (Bottom panel) position of 850 ridge lines of the time filtered motion field based on "anomaly experiment" during July 31 to August 29, 1984

is shown in Fig. 14b. Basically, a reasonable southward motion of the low frequency trough line has been predicted by this approach to almost 30 days. Is this an example where the ridge line is slowly being replaced by a trough line and a dry spell is being replaced by a wet spell of the monsoon? To answer this question we shall first look at the observational aspects. Figure 15 shows the time filtered area averaged rainfall during August and September, 1984, for northern and southern India. This is based on raingauge observations. Note the initial wet spell over northern India and a dry spell over southern India during early August and a reversal in late August, suggesting a southward passage of the wet spell along with the monsoon trough axis. The daily rainfall data were filtered on this time scale to examine if the propagation of the wet spell southwards was in-phase with the passage of the monsoonal trough-ridge wave system. In the daily precipitation series there are other time scale with significant variance, e.g., the 5–7-day oscillation associated with the passage of monsoonal depressions over northern India (Hartmann and Michelsen, 1989) during this period; hence we felt it would be difficult to detemine the phase relationship with the unfiltered series.

The upper troposphere velocity potential anomaly on this time scale exhibited an unusual

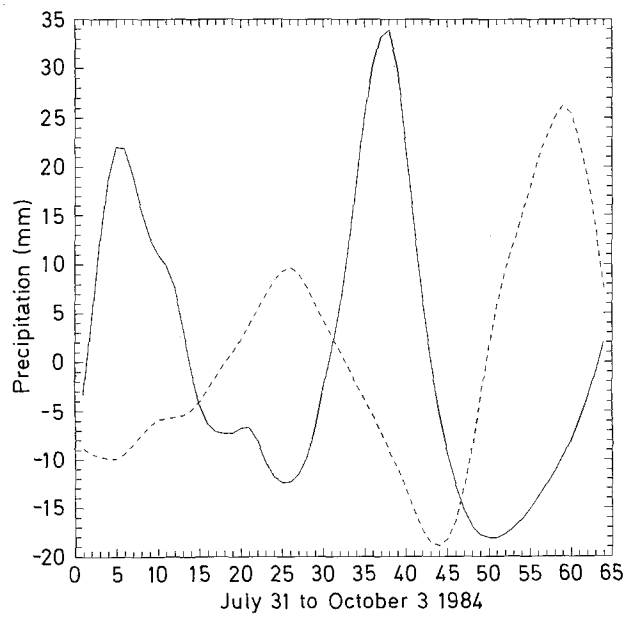

Fig. 15. Time filtered observed area averaged rainfall during August and September, 1984, for North and South India. Solid line for Northern India and dashed line for Southern India

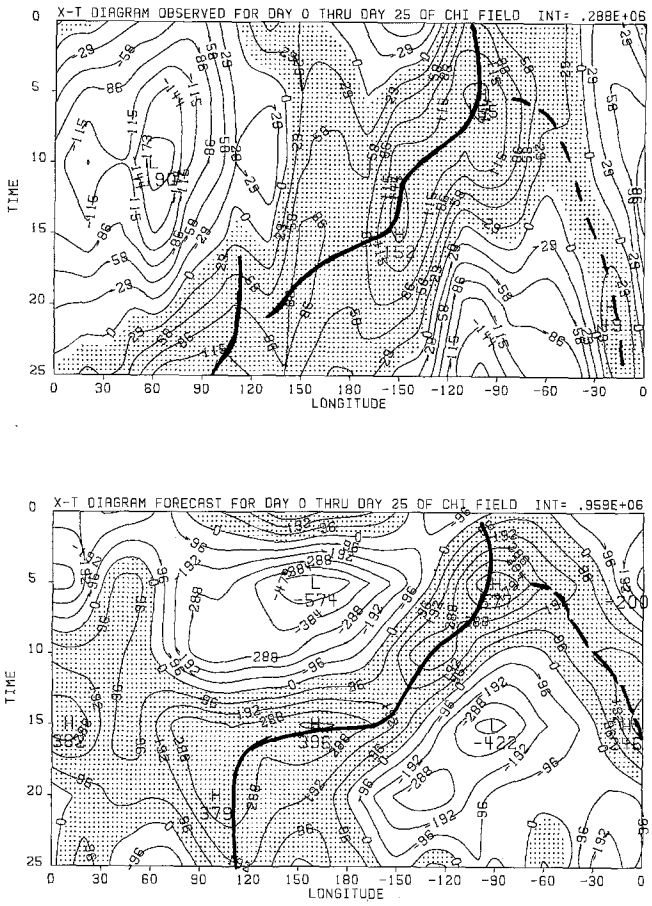

Fig. 16. An *x-t* diagram of the velocity potential anomaly averaged from 30°S to 30°N during the period July 31 to August 24, 1979. Top banel based on "observed" fields, while the bottom panel shows results from the anomaly experiment. Units $m^2 s^{-1}$

westward motion during the month of August, 1984. Figure 16 illustrates a longitude-time diagram of the meridionally averaged (from 30°S to 30°N) velocity potential based on the observed wind (top-panel) and that for the anomaly experiment (bottom panel). The anomaly experiment captures the basic westward motion of the velocity potential anomaly.

Thus, two experiments, one for 1979 exhibiting a normal motion of the low frequency waves and the other for 1984 exhibiting an anomalous behavior, have been reasonably successfully integrated to almost 30 days.

4. Concluding Remarks

In this paper we have shown a somewhat simplistic approach to extend the predictability of low frequency modes. This extension required the time

filtering of high frequency modes from the initial states of long-term integration. The model requires the specifications of a time mean state, an initial low frequency anomaly for all the fields at all the vertical levels of a global spectral model and time varying sea surface temperature anomalies specified during the entire course of integration. We have shown examples of application of the approach to the prediction of a break in the monsoon. These integrations show skill in the prediction for periods of the order of 4 weeks.

This study has raised a number of questions that require further experimentation.

a) The role of the time mean state requires further analysis. We are presently carrying out sensitivity studies by replacing the time mean state with a climatological time state to explore the sensitivity of the low frequency wave motions to the definition of the initial time mean state.

b) It is necessary to explore how we might replace the future value of the SST anomalies used in the present experiments to make this a truly predictive experiment. A possible experiment would be to define an initial anomaly and keep it fixed during an extended integration.

c) In the present experiments the energy exchange from the higher to the lower frequencies is very small during the initial 30 days of integration. Observational energetics however, do imply that the maintenance of the low frequency modes crucially depend on this energy exchange. Ways to parameterize this energy exchange in the frequency domain requires further observational studies.

d) Can the model self-generate a low frequency mode if it were excluded initially? Our feeling is that the model cannot correctly reproduce an anomaly if it is absent initially. This hypothesis needs to be explored.

We have completed a few sensitivity studies which show that: The forecasts are not very sensitive if the initial date is altered by one day. Forecasts started on August 1, 1979 and July 31, 1979 basically produced the same results. Removing the SST anomalies altogether and only retaining the annual cycle of the SST fails to provide sufficient amplitude for the low frequency modes. Such forecasts were quite poor. The SST anomalies seem to be quite important for the type of modelling effort presented here. Further work is continuing in most of these above ares.

Appendix I

An Outline of the FSU Global Model

Domain: global
Dependent variables: vorticity, divergence, temperature, dew point depression and the log of surface pressure. ζ, D, T, S, $\ln p_s$ (a list of useful symbols is given in Table 2)
Vertical coordinate: σ (8 layers)
Horizontal: spectral representation T21 (triangular truncation 21 waves)
Vertical: finite difference representation
Transform method: alias-free nonlinear advection
Time differencing: semiimplicit, Asselin time filter $\gamma = 0.5$; Asselin (1972)
Horizontal diffusion: linear (fourth order) following Kanamitsu et al. (1983)
$K = 2 \times 10^{15} \mathrm{m}^4 \mathrm{S}^{-1}$ (for ζ, T, S)
$K = 2 \times 10^{16} \mathrm{m}^4 \mathrm{S}^{-1}$ (for D)
Envelope-orography: $\bar{h} + 2$ *s.d.* based on a basic data NAVY 10 minute resolution tape
Vertical boundary conditions: kinematic, $\sigma = 0$ top and bottom
Data: ECMWF IIIb
Initialization: nonlinear normal mode with physics, 5 vertical modes; Kitade (1983)

Physical processes

Large scale condensation: disposition of supersaturation T, q
Dry convective adjustment: Kanamitsu (1975)
Shallow convection: Tiedke and Slingo (1985)
Deep moist convection: modified Kuo scheme, Krishnamurti et al. (1983)
Planetary boundary layer: surface fluxes are based on the similarity theory, vertical distribution of fluxes is Richardson number dependent
Radiative processes: long wave radiation – Band model (Harshvardhan and Corsetti, 1984)
Short wave radiation – Lacis and Handen (1974). The model includes cloud feedback processes, threshold relative humidity to define clouds; diurnal change is introduced via a variable zenith angle
Surface temperature is based on 10-day mean SST values

Table 2. *A List of Useful Symbols*

D	divergence
T	temperature
S	dew point depression
p_s	surface pressure
σ	vertical coordinate
K	horizontal diffusion coefficient
h	height of the mountain above sea level
s.d.	standard deviation
φ	geopotential height
$\tilde{\sigma}$	value of σ at an intermediate model level
s	subscript s denotes value at the earth's surface

Note: The remaining symbols are explained in the text.

over the oceans; the ground temperature is calculated from the surface energy balance over land and is coupled to surface fluxes and a surface hydrology is included, Krishnamurti et al. (1988 a)

Appendix II

Recursion Technique for 1st-order Butterworth Band-Pass Filter

The conventional method of filtering a discrete time series is by convolving the input series with the weighting function of the filter. The output series can be expressed as:

$$y_k = \sum_{i=-M}^{M} w_i x_{k-i}, \tag{1}$$

where $(x_0, x_1, \ldots, x_{N-1})$ are N values of the input series,
$(w_{-M}, w_{-M+1}, \ldots, w_M)$ are $2M+1$ values of the weighting function,
and $(y_{-M}, y_{-M+1}, \ldots, y_{N+M-1})$ are the $N+2M$ values of the output series.

Using the z-transform, the convolution operation in Eq. (1) is given by:

$$Y(z) = W(z)\,X(z) \tag{2}$$

where

$$Y(z) = \sum_{l=-M}^{N+M-1} y_l z^l$$

$$W(z) = \sum_{l=-M}^{M} w_l z^l$$

$$X(z) = \sum_{l=0}^{N-1} x_l z^l$$

Here, z, is usually a complex variable and its positive (negative) power represents delay (advance) operation in units of sampling interval (Δt). The response function $R(\omega)$ is then given by $W(e^{-i\omega\Delta t})$.

Expressing $W(z)$ as a rational function of z, i.e.,

$$W(z) = \sum_{l=0}^{n} a_l z^l \sum_{l=0}^{m} b_l z^l \tag{3}$$

and substituting it in Eq. (2) yields

$$\sum_{i=0}^{m} b_i z^i \sum_{j=-M}^{N+M-1} y_j z^j = \sum_{k=0}^{n} a_k z^k \sum_{l=0}^{N-1} x_l z^l \tag{4}$$

Equating the coefficients of the same powers of z on both sides of Eq. (4) yields

$$\sum_{j=0}^{m} b_j y_{k-j} = \sum_{i=0}^{n} a_i x_{k-i} \tag{5}$$

Now, we can set $b_0 = 1$ without any loss of generality and rewrite Eq. (5) in recursive form as:

$$y_k = \sum_{i=0}^{n} a_i x_{k-i} - \sum_{j=1}^{m} b_j y_{k-j} \tag{6}$$

To correctly specify the filtering coefficients, a_i and b_j, the rational function $W(z)$ is synthesized by the systematic transformation method of Ruston and Bordogna (1966). Here, we first define a prototype filter, commonly a low-pass filter and then through appropriate frequency transformations, this filter is transformed into a high-pass, band-pass or multi-pass filter as desired.

Following Shanks (1967), a digital band-pass filter based on a first-order Butterworth function is designed. For an n^{th}-order Butterworth function, the amplitude response function is given by

$$|W(i\omega)|^2 = \frac{1}{1+\omega^{2n}} \tag{7}$$

The first-order response function, $W(i\omega)$, may be represented on the S-plane by,

$$W(S) = \frac{1}{1+S} \tag{8}$$

The following transformation, is used to convert the low-pass to a band-pass filter,

$$S = \frac{s^2 + \Omega_0^2}{sB} \tag{9}$$

where
$\Omega_0 = \sqrt{\Omega_2 \cdot \Omega_1}$, is the geometric mean of the cut off frequencies Ω_1 and Ω_2, respectively,
and $B = |\Omega_2 - \Omega_1|$ is the bandwidth of the spectral window.

On substitution of Eq. (9) into (8) we obtain,

$$W(s) = \frac{sB}{\Omega_0^2 + sB + s^2} \tag{10}$$

The response function in the z-plane is then obtained by taking the following transformation,

$$s = \frac{2}{\Delta t}\,\frac{(1-z)}{(1+z)} \tag{11}$$

To obtain the response function, define $z = e^{-i\omega\Delta t}$, where ω is the angular frequency, and make use of Eq. (10) and (11) to obtain the following relationship.

$$W(z) = \frac{a(1-z^2)}{1 + b_1 z + b_2 z^2}, \tag{12}$$

where,

$$\begin{aligned} a &= 2\Delta\Omega/D \\ b_1 &= 2(\Omega^2 - 4)/D \\ b_2 &= (\Omega^2 - 2\Delta\Omega + 4)/D \end{aligned} \tag{13}$$

and D, Ω and $\Delta\Omega$ satisfy the following relationship

$$\begin{aligned} D &= \Omega^2 + 2\Delta\Omega + 4 \\ \Omega^2 &= \frac{4\sin\omega_1\Delta t \sin\omega_2\Delta t}{(1+\cos\omega_1\Delta t)(1+\cos\omega_2\Delta t)} \\ \Delta\Omega &= 2\,\frac{\sin\omega_1\Delta t}{1+\cos\omega_1\Delta t} - \frac{\sin\omega_2\Delta t}{1+\cos\omega_2\Delta t} \end{aligned} \tag{14}$$

where, ω_1 and ω_2 corresponds to the frequencies with a 0.5 response.

Using the coefficients from Eq. (13) in our filter the band-passed output can be computed from Eq. (6), which gives,

$$y_k = a(x_k - x_{k-2}) - b_1 y_{k-1} - b_2 y_{k-2} \tag{15}$$

Note that Eq. (5) is a recursive filter requiring only two data points in the past and two previously computed output points. In general, for a sufficient long-time series such recursive filters do not have zero or linear phase spectra. An advantage of these techniques is that it gives a rapid convergence compared to conventional filters based on weighted averages, and also we can specify the peak in the response curve at its bandwidth arbitrarily.

Appendix III

Kinetic Energy Spectra

Nonlinear Energy Transfer Spectra

The computations of the kinetic energy spectra in the frequency domains follow Hayashi (1980) and Sheng (1986).

The equations of motion and continuity in spherical coordinates (λ, θ, p) are written in flux form as;

$$\frac{\partial u}{\partial t} = \left[-\frac{\partial uu}{\partial x} - \frac{\partial uv}{\partial y} - \frac{\partial uw}{\partial p} + \frac{\tan\theta uv}{r} \right] + 2\Omega \sin\theta v - g\frac{\partial z}{\partial x} + F_u \tag{1}$$

$$\frac{\partial v}{\partial t} = \left[-\frac{\partial uv}{\partial x} - \frac{\partial vv}{\partial y} - \frac{\partial wv}{\partial p} + \frac{\tan\theta}{r} uu \right] - 2\Omega \sin\theta u - \frac{g}{r}\frac{\partial z}{\partial \theta} + F_v \tag{2}$$

$$\frac{\partial u}{\partial x} + \frac{\partial y}{\partial y} + \frac{\partial w}{\partial p} = 0 \tag{3}$$

where

$$\frac{\partial(\ )}{\partial x} = \frac{\partial(\ )}{r\cos\theta\,\partial\lambda} \tag{4}$$

$$\frac{\partial(\ )}{\partial y} = \frac{\partial \cos\theta(\ )}{r\cos\theta\,\partial\theta} \tag{5}$$

The terms in the brackets in (1) and (2) are nonlinear terms due to advection and sphericity.

At each point in space the time series data $u(t)$, $v(t)$, $w(t)$ and $z(t)$ sampled at N equally spaced time intervals of Δt (= 1 day) may be represented by a discrete time-fourier series with Nyquist frequency $\frac{1}{2\Delta t}$ as

$$u(t) = u(j\Delta t) = \sum_{n=0}^{N-1} U(n)\, e^{i2\pi uj/N}$$

where $j = 0, 1, \ldots N-1$

and $U(n) = U(f_n)$ where $f_n = \frac{n}{N\Delta t} \quad n = 0, 1, \ldots N-1$

is the Fourier transform of $u(t)$ for discrete frequency values f_n. At these frequencies the transformed components are defined by

$$U(n) = \sum_{j=0}^{N-1} u(t)\, e^{-i2\pi jn/N} \quad n = 0, 1, 2, \ldots N-1 \tag{6}$$

Since u is a real time series, we have the following relationship

$U(-n) = U^c(n)$; the complex conjugate of $U(n)$

The sample frequency cospectra $P_n[u, v]$ and quadrature cospectrum $Q_n[u, v]$ (Jenkins and Watts, 1968) are defined as

$$P_n[u,v] = \begin{cases} \tfrac{1}{2}\, Re\{U^c(n)\, V(n)\} & n = 1, 2, \ldots M \\ U(0)\, V(0) & n = 0 \end{cases} \tag{7}$$

$$Q_n[u,v] = \begin{cases} \tfrac{1}{2}\, Im\{U^c(n)\, V(n)\} & n = 1, 2, \ldots M \\ 0 & n = 0 \end{cases} \tag{8}$$

where M is equal to $\left[\frac{n-1}{2}\right]$, Re and Im denote the real and imaginary parts respectively.

The sample cospectrum is interpreted as the spectrum of the sample covariance averaged over time as

$$\overline{u(t)\, v(t)} = \sum_{n=0}^{M} P_n[u, v]$$

The sample quadrature cospectrum is interpreted as the cospectrum between u and v with a 90° phase shift

More, generally, the sample cross spectra $R_n[u, v]$ are defined as

$$R_n[u,v] = P_n[u,v] + i\, Q_n[u,v] \tag{9}$$

In terms of the frequency cospectrum, the kinetic energy per unit mass $K(n)$ for the frequency n is defined by

$$K(n) = \tfrac{1}{2}\,[P_n[u,u] + P_n[v,v]] \quad n = 0, 1, 2, \ldots, M \tag{10}$$

To obtain the kinetic energy spectra, take a cospectrum operation between u (or v) and both sides of Eq. (1) (or 2) and make use of the continuity equation to yield:

$$\begin{aligned} P_n\left[u, \frac{\partial u}{\partial t}\right] = &-\left[P_n\left[u, \frac{\partial uu}{\partial x}\right] + P_n\left[u, \frac{\partial vu}{\partial y}\right] \right. \\ &\left. + P_n\left[u, \frac{\partial wu}{\partial p}\right] - \frac{\tan\theta}{r} P_n[u, uv] \right] \\ &+ 2\Omega \sin\theta\, P_n[u, v] - P_n\left[u, g\frac{\partial z}{\partial x}\right] \\ &+ P_n[u, F_u] \\ &= 0 \end{aligned} \tag{11}$$

$$\begin{aligned} P_n\left[v, \frac{\partial v}{\partial t}\right] = &-\left[P_n\left[v, \frac{\partial uv}{\partial x}\right] + P_n\left[v, \frac{\partial vv}{\partial y}\right] \right. \\ &\left. + P_n\left[v, \frac{\partial wv}{\partial p}\right] + \frac{\tan\theta}{r} P_n[v, uu] \right] \\ &- 2\sin\theta\, P_n[v, u] - P_n\left[v, \frac{g}{r}\frac{\partial z}{\partial \theta}\right] \\ &+ P_n[v, F_v] \\ &= 0 \end{aligned} \tag{12}$$

The terms $P_n\left[u, \frac{\partial u}{\partial t}\right]$ and $P_n\left[v, \frac{\partial v}{\partial t}\right]$ vanish, since

$$P_n\left[u, \frac{\partial u}{\partial t}\right] = -\frac{2\pi n}{N\Delta t} Q_n[u, u]$$

$$P_n\left[v, \frac{\partial v}{\partial t}\right] = -\frac{2\pi n}{N\Delta t} Q_n[v, v]$$

and by Eq. (8) $Q_n[u, u] = Q_n[v, v] = 0$.

The spectral kinetic energy equation is then obtained by adding Eqs. (11) and (12)

$$\begin{aligned} 0 = &- P_n\left[u, \frac{\partial uu}{\partial x}\right] + P_n\left[u, \frac{\partial vu}{\partial y}\right] + P_n\left[u, \frac{\partial wu}{\partial p}\right] \\ &+ P_n\left[v, \frac{\partial uv}{\partial x}\right] + P_n\left[v, \frac{\partial vv}{\partial y}\right] + P_n\left[v, \frac{\partial wv}{\partial p}\right] \\ &+ \frac{\tan\theta}{r}[P_n[u, uv] - P_n[v, uu]] \\ &- P_n\left[u, g\frac{\partial z}{\partial x}\right] - P_n\left[v, \frac{g}{r}\frac{\partial z}{\partial \theta}\right] \\ &+ P_n[u, F_u] + P_n[v, F_v] \end{aligned} \tag{13}$$

Now, by the definition of the cross-spectra and making use of the continuity and hydrostatic equations, the following relationship is obtained.

$$\begin{aligned} &-\left[P_n\left[u, g\frac{\partial z}{\partial x}\right] + P_n\left[v, \frac{g}{r}\frac{\partial z}{\partial \theta}\right]\right] \\ &= -g\left[\frac{\partial}{\partial x}P_n[u, z] + \frac{\partial}{\partial y}P_n[v, z]\right. \\ &\quad \left. - P_n\left[\frac{\partial u}{\partial x}, z\right] - P_n\left[\frac{\partial v}{\partial y}, z\right]\right] \\ &= -g\left[\frac{\partial}{\partial x}P_n[u, z] + \frac{\partial}{\partial y}P_n[v, z]\right. \\ &\quad \left. + \frac{\partial}{\partial p}P_n[w, z] - P_n\left[w, \frac{\partial z}{\partial p}\right]\right] \\ &= -g\left[\frac{\partial}{\partial x}P_n[u, z] + \frac{\partial}{\partial y}P_n[v, z]\right. \\ &\quad \left. + \frac{\partial}{\partial p}P_n[w, z] - P_n[w, a]\right] \end{aligned} \tag{14}$$

Thus, the final form of the kinetic energy equation in the frequency domain is written as

$$\begin{aligned} 0 &= \langle K \cdot K(n)\rangle - P_n[w, a] \\ &= -g\left[\frac{\partial}{\partial x}P_n[u, z] + \frac{\partial}{\partial y}P_n[v, z] - \frac{\partial}{\partial p}P_n[w, z]\right] \\ &\quad - \{P_n[u, F_u] + P_n[v, F_v]\} \end{aligned} \tag{15}$$

The nonlinear kinetic energy transfer spectrum $\langle K \cdot K(n)\rangle$ in (15) is defined by

$$\begin{aligned} \langle K \cdot K(n)\rangle = &-\left[P_n\left[u, \frac{\partial}{\partial x}uu\right] + P_n\left[u, \frac{\partial}{\partial y}vu\right]\right. \\ &+ P_n\left[u, \frac{\partial}{\partial p}wu\right] + P_n\left[v, \frac{\partial}{\partial x}uv\right] \\ &\left. + P_n\left[v, \frac{\partial}{\partial y}vv\right] + P_n\left[v, \frac{\partial}{\partial p}wv\right]\right] \\ &+ \frac{\tan\theta}{r}[P_n[u, uv] - P[v, uu]] \end{aligned} \tag{16}$$

According to Fjortoft (1953), a nonlinear transfer of kinetic energy into or from an intermediate frequency mode occurs via a three-way interaction between modes having frequencies n, $(n \pm m)$ and m respectively, such that the following relation is satisfied.

$$n = (n \pm m) \mp m$$

$\langle K \cdot K(n)\rangle$ can be further partitioned into two parts as

$$\langle K \cdot K(n)\rangle = \langle K(m) \cdot K(n)\rangle + \langle K(0) \cdot K(n)\rangle \tag{17}$$

where $\langle K(m) \cdot K(n)\rangle$ is the transfer of energy into frequency n by interaction among different frequencies excluding 0 (time mean). While $\langle K(0) \cdot K(n)\rangle$ is the transfer of energy into frequency n by interaction between the stationary (time mean) flow and frequency n.

By definition, $\langle K(m) \cdot K(n)\rangle$ is given as

$$\begin{aligned} \langle K(m) \cdot K(n)\rangle = &- P_n\left[u, \frac{\partial u'u'}{\partial x}\right] + P_n\left[u, \frac{\partial v'u'}{\partial y}\right] \\ &+ P_n\left[u, \frac{\partial w'u'}{\partial p}\right] + P_n\left[v, \frac{\partial u'v'}{\partial x}\right] \\ &+ P_n\left[v, \frac{\partial v'v'}{\partial y}\right] + P_n\left[v, \frac{\partial w'v'}{\partial p}\right] \\ &+ \frac{\tan\theta}{r}[P_n[u, u'v'] - P_n[v, u'u']] \end{aligned} \tag{18}$$

The interaction between the stationary (time mean) and transient motions is given as a residual by

$$\langle K(0) \cdot K(N)\rangle = \langle K \cdot K(m)\rangle - \langle K(m) \cdot K(n)\rangle$$

Sheng (1986) has shown that this residual is not a small difference of large numbers. Moreover, $\langle K(0) \cdot K(n)\rangle$ can be computed explicitly from linearized equations as follows

$$\begin{aligned} \langle K(0) \cdot K(n)\rangle = &-\left[\frac{\partial \bar{u}}{\partial x}P_n[u, u] + \frac{1}{r}\frac{\partial \bar{u}}{\partial \theta}P_n[u, v]\right. \\ &+ \frac{\partial u}{\partial p}P_n[u, v] + \frac{\partial \bar{v}}{\partial x}P_n[u, v] \\ &\left. + \frac{1}{r}\frac{\partial \bar{v}}{\partial \theta}P_n[v, v] + \frac{\partial \bar{v}}{\partial p}P_n[w, v]\right] \\ &- \left[\frac{\partial \bar{u}K(n)}{\partial x} + \frac{\partial \bar{v}K(n)}{\partial y} + \frac{\partial \bar{w}K(n)}{\partial p}\right] \end{aligned} \tag{19}$$

In computing the nonlinear kinectic energy transfers we neglected the terms involving the vertical derivatives in Eq. (18) and (19) as their contributions are small compared to the remaining terms.

Acknowledgements

We are indebted to Ms. Rosemarie Raymond and Janie Nall for technical assistance in the preparation of this work. The research reported here was supported equally by two grants to the Florida State University, NSF Grant No. ATM-8812053 and NOAA Grant No. NA 87 AA-D-AC038. The authors acknowledge the San Diego Supercomputer Center which is sponsored by the National Science Foundation, for the computing time used in this research.

References

Asselin, R., 1972: Frequency filter for time integrations. *Mon. Wea. Rev.*, **100**, 487–490.

Browning, G. L., Hack, J. J., Swarztrauber, P. N., 1989: A comparison of three numerical methods for solving differential equations on the sphere. *Mon. Wea. Rev.*, **117**, 1058–1075.

Daley, R. C., Girard, C., Henderson, J., Simmonds, I., 1976: Short-term forecasting with a multi-level spectral primitive equation model. Part 1: Model formulation. *Atmosphere*, **14**, 98–116.

Fjortoft, R., 1953: On the changes in the spectral distribution of kinetic energy for tow-dimensional, non-divergent flow. *Tellus*, **5**, 225–230.

Harshvardhan, Corsetti, T. G., 1984: Longwave parameterization for the UCLA/GLAS GCM. NASA Tech. Mem. 86072, Goddard Space Flight Center, Greenbelt, MD 20771.

Hartmann, D. L., Michelsen, M. L., 1989: Intraseasonal periodicties in Indian rainfall. *J. Atmos. Sci.*, **46**, 2838–2862.

Hayashi, Y., 1980: Estimation of nonlinear energy transfer spectra by the cross-spectral method. *J. Atmos. Sci.*, **37**, 299–307.

Jenkins, G. M., Watts., D. G., 1968: *Spectral Analysis and Its Applications*. San Francisco: Holden-Day, 525 pp.

Kanamitsu, M., 1975: On numerical prediction over a global tropical belt. Report No. 75-1, pp. 1–282. (Available from the Dept. of Meteorology, Florida State University, Tallahassee, FL 32306, U.S.A.)

Kanamitsu, M., Tada, K., Kudo, K., Sato, N., Isa, S., 1983: Description of the JMA operational spectra model. *J. Meteor. Soc. Japan*, **61**, 812–828.

Kitade, T., 1983: Nonlinear normal mode initialization with physics. *Mon. Wea. Rev.*, **111**, 2194–2213.

Krishnamurti, T. N., Subrahmanyam, D., 1982: The 30–50 day mode at 850 mb during MONEX. *J. Atmos. Sci.*, **39**, 2088–2095.

Krishnamurti, T. N., Low-Nam, S., Pasch, R., 1983: Cumulus parameterization and rainfall rates II. *Mon. Wea. Rev.*, **111**, 815–828.

Krishnamurti, T. N., Jayakumar, P. K., Sheng, J., Surgi, N., Kumar, A., 1985: Divergent circulations on the 30 to 50 day time scale. *J. Atmos. Sci.*, **42**, 364–375.

Krishnamurti, T. N., Bedi, H. S., Heckley, W., Ingles, K., 1988 a: Reduction of the spin up time for evaporation and precipitation in a spectral model. *Mon. Wea. Rev.*, **116**, 907–920.

Krishnamurti, T. N., Oosterhof, D. K., Mehta, A. V., 1988 b: Air-sea interaction on the time scale of 30–50 days. *J. Atmos. Sci.*, **45**, 1304–1322.

Krishnamurti, T. N., Oosterhof, D. K., 1989: Prediction of the life cycle of a supertyphoon with a high resolution global model. *Bull. Amer. Meteor. Soc.*, **70**, 1218–1230.

Lacis, A. A., Hansen, J. E., 1974: A parameterization for the absorption of solar radiation in the earth's atmosphere. *J. Atmos. Sci.*, **31**, 118–133.

Lorenc, A. C., 1984: The evolution of planetary scale 200 mb divergences during the FGGE year. *Quart. J. Roy. Meteor. Soc.*, **110**, 427–442.

Mehta, A. V., Krishnamurti, T. N., 1988: Interannual variability of the 30 to 50 day wave motions. *J. Met. Soc. Japan*, **66**, 535–548.

Ruston, H., Bordogna, J., 1966: *Electric Networks: Functions, Filters, Analysis*. New York: McGraw-Hill, 552 pp.

Saltzman, B., 1970: Large-scale atmospheric energetics in the wave number domain. *Rev. Geophys. Space Phys.*, **8**, 829–302.

Shanks, J., 1967: Recursion filters for digital processing. *Geophysica*, **32**, 33–51.

Sheng, J., 1986: On the energetics of low frequency motions. Ph.D. Dissertation. (Available from the Department of Meteorology, Florida State University, Tallahassee, FL 32306, U.S.A.)

Tiedke, M., Slingo, J., 1985: Development of the operational parameterization scheme. ECMWF Research Dept. Tech. Memo No. 108, 38 pp. (Available from ECMWF, Shinfield Park, Reading, Berkshire RG2 9AX, England.)

Wallace, J. M., Tibaldi, S., Simmons, A. J., 1983: Reduction of systematic forecast errors in the ECMWF model through the introduction of envelope orography. *Quart. J. Roy. Meteor. Soc.*, **109**, 683–718.

Yasunari, T., 1980: A quasi-stationary appearane of 30 to 40 day period in the cloudiness fluctuations during the summer monsoon over India. *J. Meteor. Soc. Japan*, **58**, 225–229.

Yasunari, T., 1981: Structure of an Indian summer monsoon system with around 40-day. *J. Meteror. Soc. Japan*, **59**, 336–354.

Authors' address: T. N. Krishnamurti, M. Subramaniam, D. K. Oosterhof, and G. Daughenbaugh, Department of Meteorology, Florida State University, Tallahasse, FL 32306, U.S.A.